HHS Public Access

Author manuscript

J Biomech. Author manuscript; available in PMC 2018 May 03.

Published in final edited form as:

J Biomech. 2017 May 03; 56: 19–25. doi:10.1016/j.jbiomech.2017.02.017.

A modelling approach demonstrating micromechanical changes in the tibial cemented interface due to in vivo service

Priyanka Srinivasan[1], **Mark A. Miller**[2], **Nico Verdonschot**[1,3], **Kenneth A. Mann**[2], and **Dennis Janssen**[1]

[1]Radboud university medical center, Radboud Institute for Health Sciences, Nijmegen, The Netherlands [2]Department of Orthopedic Surgery, State University of New York, Upstate Medical University, Syracuse, New York, USA [3]University of Twente, Laboratory for Biomechanical Engineering, Faculty of Engineering Technology, Enschede, The Netherlands

Abstract

Post-operative changes in trabecular bone morphology at the cement-bone interface can vary depending on time in service. This study aims to investigate how micromotion and bone strains change at the tibial bone-cement interface before and after cementation. This work discusses whether the morphology of the post-mortem interface can be explained by studying changes in these mechanical quantities. Three post-mortem cement-bone interface specimens showing varying levels of bone resorption (minimal, extensive and intermediate) were selected for this study Using image segmentation techniques, masks of the post-mortem bone were dilated to fill up the mould spaces in the cement to obtain the immediately post-operative situation. Finite element (FE) models of the post-mortem and post-operative situation were created from these segmentation masks. Subsequent removal of the cement layer resulted in the pre-operative situation. FE micromotion and bone strains were analyzed for the interdigitated trabecular bone. For all specimens micromotion increased from the post-operative to the post-mortem models (distally, in specimen 1: 0.1 to 0.5 μm; specimen 2: 0.2 to 0.8 μm; specimen 3: 0.27 to 1.62 μm). Similarly bone strains were shown to increase from post-operative to post-mortem (distally, in specimen 1: −185 to −389 με; specimen 2: −170 to −824 με; specimen 3: −216 to −1024 με). Post-mortem interdigitated bone was found to be strain shielded in comparison with supporting bone indicating that failure of bone would occur distal to the interface. These results indicate that stress shielding of interdigitated trabeculae is a plausible explanation for resorption patterns observed in post-mortem specimens.

For correspondence: Priyanka Srinivasan, Orthopaedic Research Lab, Radboud university medical center, Huispost 547, PO Box 9101, 6500 HB Nijmegen, The Netherlands, priyanka.srinivasan@radboudumc.nl, Tel: +31 24 3613554, Fax: +31 24 3540555.

Conflict of interest statement

None of the authors have financial or personal relationships with other people or organizations that could inappropriately influence or bias the currently presented work.

1. Introduction

Implant loosening remains one of the most common causes for knee arthroplasty revisions (Sharkey, Lichstein et al. 2014; SKAR Annual Report 2016). While bone cement provides for stable fixation between the trabecular bone and implant, it also results in stress-shielding of the bone that is interdigitated with cement (Zhang, Cossey et al. 2016). Trabecular bone distal to metal-backed tibial trays has been shown to be more stress shielded than all-polyethylene implants using computational modeling (Thompson, Yohuno et al. 2015). Changes in peri-prosthetic tibial bone density may not always lead to complications, with good clinical outcomes achievable (Jaroma, Soininvaara et al. 2016). The importance of the cement-bone interface in achieving stable initial fixation cannot however be understated. Micromotion following *in vivo* service, which is a predictor for revision arthroplasty, has been inversely correlated with the amount of initial cement-bone interlock (Miller, Terbush et al. 2014). Recent experimental studies have shown that the cement-trabecular bone interface around tibial knee implants changes post-operatively. Different patterns of bone resorption, remodeling and fibrous tissue formation were observed in tibial component retrieval specimens. Specimens showed areas of bone resorption in the interdigitated region with bone remaining embedded deeper within the cement mantle. This observation was also accompanied by pedestal formation in which the supporting bone had remodeled to form supporting structures underneath the cement border. The interlock between cement and trabecular bone decreased with time in service (Miller, Goodheart et al. 2014).

In a previous study simulating lab-prepared cement-bone interface specimens, we analyzed the effect of the cement layer on the strain distribution in the interdigitated bone, and quantified micromotion at the cement-bone interface (Srinivasan, Miller et al. 2016). These simulations demonstrated a significant effect of the addition of a cement layer on the predicted strains in the trabecular bone, suggesting strain adaptive remodeling as a possible stimulus driving the resorption seen in post-mortem retrievals.

In the current study we aim to show how post-operative changes influence micromotion and strains in the interlocked bone using post-mortem retrieved cement-bone interface specimens. We also ask whether the interdigitated bone in post-mortem specimens is strain-shielded compared to the underlying supporting bone. We further aim to study whether bone resorption patterns observed in post-mortem specimens can be explained by micromotion and strain values obtained using finite element (FE) models. The mechanisms leading to tibial bone resorption are of particular interest, as better insights into the processes involved could potentially lead to improvements in implant design and/or changes in surgical technique.

2. Materials and Methods

2.1 Specimen description

Three cement-trabecular bone specimens (having average dimensions 9×8×11 mm) were obtained from post-mortem retrieved total knee arthroplasty donor samples. The donor samples varied in patient age, gender and time in service. The specimens obtained also varied in depth of cement penetration (Table 1). The three interface specimens showed

differing degrees and patterns of bone resorption. Specimen 1 showed the least amount of bone resorption in the interdigitated region (Fig 1a) whereas specimen 2 had almost no surviving interdigitated bone (Fig 1b). The specimen with the thickest cement penetration depth showed proximally embedded bone deep within the cement layer and substantial resorption centrally within the cement layer (Fig 1c).

2.2 Post-mortem and post-operative FE model generation

Based on micro-CT images (16 μm voxel resolution), three different models were created for each of the three cement-bone interface specimens. First, the micro-CT data was filtered using a discrete Gaussian filter (variance of 2 and maximum kernel width of 1) and segmented based on an image greyscale ranging from −1024 to −769 (Mimics 14.0, Materialise Europe, Belgium). The post-mortem bone mask was obtained using a threshold between −870 to −769. The cement mask was obtained using a threshold between −920 to −880. Some further editing of this cement mask was required (using cavity fill and Boolean operations) to eliminate inclusion of any trabecular spaces in the supporting bone. These masks were subsequently used to create models representing the post-operative situation, using the following approach. The gaps in the cement indicate the geometry of the trabeculae at the time of implant cementation (Mann, Miller et al. 2012). Through step-wise dilation of the post-mortem bone mask, the gaps in the cement layer were filled incrementally until the post-operative situation was obtained (Fig 2). After each dilation step, masks of the cement and trabecular spaces in the supporting bone were subtracted from the dilated bone mask. This procedure resulted in a restoration of the resorbed bone in the interdigitated region. In each incremental bone mask obtained in this manner, the volume of the interdigitated bone increases and trabecular connections are reformed. For specimen 2, which had extensive resorption, there was almost no post-mortem interdigitated bone to start the dilation process. The post-operative model for this specimen was simply created using Boolean operations on the cement and bone mask with a mask of the entire specimen scan set. All segmentation masks were cropped to 4.5 × 4.5 × 8 mm to limit the final size of the finite element models and computational costs. To create finite element models of each specimen, the segmentation masks of the cement, interdigitated bone and supporting bone were used to create corresponding surface and subsequently 4-node tetrahedral solid meshes (3-matic 5.1 and Patran Mesher in Mentat 2012, MSC Software Corporation, Santa Ana, CA, USA). Due to the variation in cement interdigitation depth and resorption levels between specimens, the total number of elements in the (post-operative) models ranged from 5.3 to 9.8 million with 1.4 to 2.6 million nodes. The element density was kept sufficiently high such that the micro-structure of the trabeculae was accurately represented. Where the minimum trabecular thickness was approximately 0.05 mm, the element edges were kept significantly lower than this thickness (~ 0.01 mm). Average element edge length was about 0.03 mm for all models.

In one particular specimen (3), showing higher resorption levels in the middle of the interdigitated region and embedded bone deeper within the cement, two intermediate steps between the post-mortem and post-operative scenario were modeled as well, representing different stages of bone resorption within the same specimen. For this specimen, four FE models (Fig 3) were created from the cement and bone masks described above (Mimics 14.0

and 3-matic 5.1 software, Materialise Europe, Belgium). Using the post-mortem and post-operative models, volumes of interdigitated bone were obtained to study how much addition (or inverse resorption) of bone occurred between these models.

2.3 Pre-operative FE model generation

In order to evaluate the change in strains due to implant cementation, we also recreated the pre-operative situation. For this purpose, the cement was removed from the post-operative model (Fig 4a) while retaining the top-most part of the cement layer to allow for a similar load application between the different models. This was done by cutting through the surface mesh of the cement (Rhinoceros 5.0) with a cutting plane. The cut was performed such that just enough of the interdigitated cement geometry was preserved to form a pressure plate for the trabecular bone below (Fig 4b). The surface mesh of the cement pressure plate was converted to a solid tetrahedral mesh. The three new models without interdigitated cement represented the pre-operative situation. The same boundary conditions as in the interface models were applied to these models. The element numbering for the bone was retained from the post-operative models to facilitate the calculation of change in strains.

Bone and cement were modeled as isotropic linear-elastic materials. Young's modulus for bone was set to 14 GPa and for cement 3 GPa. Poisson's ratio of 0.3 was used for both materials. All models were loaded in compression to 1 MPa (equivalent to the peak loads during level walking) and a contact analysis was performed using MSC Marc 2012 (MSC Software Corporation, Santa Ana, CA, USA). Micromotion between the interlocked trabeculae and cement was calculated using pairs of bone-cement contact nodes.

2.4 Regions of Interest (ROI) interdigitated bone

To enable post-processing of relevant output variables, the elements and nodes of the interdigitated bone within each model were divided into four regions of interest of equal thickness (Fig 5). Due to the variation in depth of cement penetration between the three post-mortem specimens, the thickness of the regions between the three post-mortem models was different. Specimen 1 had ROIs with thickness 0.6 mm; specimen 2 with 0.8 mm and specimen 3 with 1.1 mm. Regions were numbered 1–4, from most proximal to distal. The same regions of interest were defined in the post-operative and pre-operative models to facilitate comparison. Elemental strains and micromotion data were outputted using a subroutine. Median micromotion and strains were determined in each ROI and also as a function of interdigitation depth. Post-mortem strains in the interdigitated bone were compared with supporting bone strains.

3. Results

3.1 Distribution of micromotion in interdigitated bone

The results of the simulations with the original post-mortem (×) models indicated that within each specimen micromotion decreased with increasing penetration depth (Fig 6). The morphology of the three post-mortem specimens could explain the differences in relative magnitude of micromotion between specimens. By filling up the cement cavities with bone, simulating the direct post-operative situation (◆), the micromotions decreased dramatically.

3.2 Distribution of strains in interdigitated bone

Median principal compressive strains in each region as a function of the interdigitation depth are shown in Figure 7 for all three cases (post-mortem, post-operative and pre-operative). Interdigitated bone strains in the post-mortem models (×) showed an increasing trend from proximal ROI 1 through distal ROI 4. Specimen 3 (intermediate resorption), which showed considerable bone trapped deeper within the cement layer (ROI 1–2) and no trabecular connectivity with more distal bone (ROI 3–4), had very low strain proximally. The post-mortem strains tend to be higher than the pre-operative ( ) and post-operative (◆) cases in the more distal ROIs. This could be explained by the fact that bone has been resorbed leading to higher micromotion.

3.3 Interdigitated and supporting bone strain

Strain data for all four regions of the interdigitated bone in the post-mortem models were compared with the immediately distal supporting bone. The thickness of the supporting bone chosen was similar to the four ROIs; where there was large volume of overlap between ROIs 3 and 4 and supporting bone, only the overlapping supporting bone was used (Specimen 2). Results showed that the interdigitated bone was strain shielded compared to the supporting bone (Fig 8). In all cases the median strains for the four interdigitated regions and the supporting bone region were found to be significantly different using the Kruskal-Wallis test ($p < 0.01$).

3.4 Changes in strain pattern from pre-operative to post-operative

Post-operative strains were low throughout the interdigitated bone in all specimens due to the presence of the cement layer which shields the bone from the carrying load in a physiological manner. The pre-operative strains indicate this mechanism as these strains are higher in comparison with the post-operative situation (Fig 7). In general, when comparing the post-operative and pre-operative models, we see that the difference in strains in the proximal regions is higher than in the more distal regions. Assuming that bone resorption is driven by strain shielding, this would indicate that maximum bone resorption occurs at ROI 1 and the least at ROI 4.

3.5 Progressive changes in micromotion and strain

To study how the micromotions and strains change within the same specimen due to resorption of bone over time, two additional models were created for specimen 3 (intermediate bone resorption). Morphology of the post-mortem specimen showed that trabeculae deeply embedded in the cement layer (ROI 1) remained largely unresorbed and there was little to no connection with trabeculae in underlying regions (Fig 5). Median micromotion in the four regions reflected these findings, as there was minimal micromotion in ROI 1 and 2 (Fig 9a). In comparison, more distal bone (ROI 3 and 4) showed a sharp increase in micromotion. When bone was added (resorption phase 1 and 2 models), thereby restoring trabecular connections in ROI 2 and 3, median micromotion and compressive strains (Fig 9b) reduced considerably in ROI 3 and 4. The median compressive strains for the post-mortem model matched the micromotion pattern, showing higher strains in ROI 3 and 4 (1161 and 1024 με) compared with ROI 1 and 2 (108 and 101 με). The two resorption

phase models showed similar reduction in strain in the distal ROI 3 and 4 compared with the post-mortem model. The pre-operative bone model showed that median strains in the bone prior to cementation were higher in ROI 1, 2 and 3 compared with the post-operative situation. The total volume of resorbed bone, which is the difference between post-operative bone and post-mortem bone model, in the 4 ROIs is 31 %, 88 %, 87 % and 57 %.

4. Discussion

Our results show that micromotions and strain in post-mortem cement-bone interface specimens vary greatly within the different regions of interdigitation. Both micromotion and strain decrease with increasing interdigitation depth. Making use of segmentation methods, in this study we demonstrate how resorbed trabecular bone can be restored in post-mortem bone-cement specimens by using the cement as a mould of post-operative interdigitated trabeculae. On restoring bone in post-mortem specimens to obtain the morphology of the cement-bone interface in the directly post-operative situation, results from our finite element models show that trabecular bone is strain shielded in the immediately post-operative situation.

Micromotion predicted in our post-mortem model of specimen 2 showing extensive resorption is lower than that for specimen 3 with intermediate resorption (Fig 6). This is counterintuitive to what might be expected with greater bone resorption, but can probably be explained by the manner in which bone remodeling has occurred. Pedestal formations at the base of the cement are essentially holding the cement layer up, whereby there is relatively little motion in x-z plane, i.e. perpendicular to the loading direction, resulting in reduced overall micromotions. The post-mortem specimen with minimal resorption (specimen 1) shows the lowest micromotion compared to the other two specimens, as would be expected.

For specimen 3 (intermediate resorption), when comparing the pre-operative model to the post-operative one, we see that the difference in median strains in ROI 2 and 3 (411 and 386 με) is higher than in ROI 4 (41 με) – indicating that trabeculae in ROI 2 and 3 are strain shielded (Fig 7c). ROI 1 also shows evidence of strain shielding (median difference is 377 με). These results would indicate that bone would resorb from ROI 1–3 while ROI 4 would remain unchanged, corresponding with the volume of bone added between the post-mortem and post-operative models in ROI 1, 2 and 3.

Comparison of strain results for post-operative and pre-operative models show that the bone in the proximal layers becomes strain-shielded post-operatively (Fig 7). In the case of specimen 3, the fact that trabecular bone in ROI 1 is not resorbed and remains embedded could possibly be explained by the (lack of) vascularity of the bone-cement interface. There may be no means for entrapped bone to be removed by fluid/cell interaction. The cement penetration depth may also play a role in the resulting resorption pattern. Higher micromotion observed distally could play a part in facilitating bone resorption by aiding in the fluid pumping mechanism around the interface.

Analysis of interdigitated and supporting bone strains for the post-mortem FE models showed that in all three specimens the supporting bone strain was higher than in ROI 4. This

would indicate that the bone would be most likely to fail in the region distal to the cement-bone interface and not within the interdigitated region. Experimental tests of post-mortem retrieved tibias under physiological loads have also shown that strains are higher below the interface compared to further distally (Zimmerman, Miller et al. 2016).

The work presented here has some limitations with regards to the methodology. This study has three specimens, each having different levels of bone resorption as well as different cement penetration depths. The influence of each variable could not be studied independently. The specimens were all loaded in compression whereas the peri-implant tibial bone might be subjected to shear and/or a combination of loads depending on the location below the implant and around the keel (if present). Resorption patterns may also vary spatially over the tibial interface. FE models of the specimens had to be cut down in size as the complex contact surfaces result in computationally demanding and time consuming simulations. The results for micromotion and strain do however show consistency in the pattern observed.

The method adopted here to restore resorbed bone to obtain the two additional models representing phases of resorption is somewhat artificial in nature, as the existing post-mortem bone is simply dilated incrementally irrespective of direction (proximal/distal). The volume of added bone was used to choose the intermediate resorption-phase models. This approach may not fully represent a realistic reversal of the bone resorption process over time, as bone resorption could occur non-linearly in terms of bone volume and spatial distribution with *in vivo* service. This could be improved upon by using strain/stimulus based resorption algorithms which would provide a more realistic resorption pattern as bone tissue has been shown to adapt its morphology towards uniform loading (Christen, Van Rietbergen et al. 2012; Christen, Ito et al. 2013). Such approaches have previously been used in other micro- and macro-scale studies on bone remodeling of trabecular bone. Ruimerman *et al* have used mechanical loading and strain energy based osteocyte stimulation to obtain altered bone architecture and subsequent homeostasis (Ruimerman, Van Rietbergen et al 2003; Ruimerman, Van Rietbergen et al 2005). Other researchers have also shown that bone remodeling in animals (Schulte, Ruffoni et al 2013) and humans (Christen, Ito et al 2014) alike is regulated by loading at the tissue level and have demonstrated that there is no lazy zone as previously thought. Osteoporotic changes in whole vertebral micro-FE models have also been simulated using a load-adaptive remodeling algorithm with a resultant loss of bone tissue (Badilatti, Christen et al 2016). At the macroscopic level, the anisotropy of bone cannot be modeled as closely as at the microscopic level as micro-FE models capture the rod and plate-like morphology of trabecular bone. Bone density information has previously been used to predict in vivo bone loading which can then be used to determine changes in morphology where information about the actual in vivo loading is limited (Weinans, Huiskes et al 1992, Fischer, Jacobs et al 1995). More recently, contact simulations have been used to obtain more realistic *in vivo* joint loads which served as input for density-based load estimation methods (Bona, Martin et al 2006). Adopting the aforementioned methods to our post-operative models to obtain intermediate resorption-phase models might offer more reliable results. The results obtained from our resorption phase models might then show different values for micromotions and strain, but we expect that the general trends observed using our method would remain the same. Furthermore, in our models we do not take into

consideration that the supporting bone has gone through remodeling as well and possibly some resorption after cementation of the implant and during *in vivo* service. The supporting bone was left unchanged in the post-operative and pre-operative models, retaining the same geometry as in the post-mortem models. Interdigitated strains predicted by the FE models could be affected by this limitation. Nevertheless the observed trends for bone strain and micromotions would still hold.

We did not apply this segmentation method to create resorption phase models for the other two specimens in this study. Applying this method to the specimen with little resorption would not have resulted in any additional information as the quantity of bone being added at intermediate resorption phases would be insignificant. The method proposed here for the specimen with extensive resorption was not feasible due to the lack of any interdigitated bone within the cement layer.

Our results indicate that stress shielding of trabeculae within the interdigitated bone is a plausible explanation for the bone resorption observed in post-mortem specimens. This implies that the use of bone cement as an implant-fixation method will, to some extent, always result in loosening of the cement-trabecular interlock over time. The ultimate goal of a successful joint reconstruction is that the implant remains stably fixed throughout the lifetime of the patient, without the need for a revision surgery. Having recognized that cemented fixation will result in peri-prosthetic bone remodeling and possible resorption of the interdigitated bone, it is important to study what factors could lead to potential failure of the of the reconstruction. In other words, what changes can be made such that failure of the reconstruction even with a compromised cement-bone interface does not occur. Future work will revolve around studying the influence of surgical factors such as the use of anchoring holes and peripheral or keel cementing only and implant related factors such as low stiffness designs and keel length.

Acknowledgments

Research reported in this publication was supported by the National Institute of Arthritis and Musculoskeletal and Skin Diseases of the National Institutes of Health under Award Number AR42017. The content is solely the responsibility of the authors and does not necessarily represent the official views of the National Institutes of Health.

References

Badilatti SD, Christen P, Parkinson I, Müller R. Load-adaptive bone remodeling simulations reveal osteoporotic microstructural and mechanical changes in whole human vertebrae. J Biomech. 2016; 49(16):3770–3779. [PubMed: 27793404]

Bona MA, Martin LD, Fischer KJ. A contact algorithm for density-based load estimation. J Biomech. 2006; 39(4):636–644. [PubMed: 16439233]

Christen P, van Rietbergen B, Lambers FM, Müller R, Ito K. Bone morphology allows estimation of loading history in a murine model of bone adaptation. Biomech Model Mechanobiol. 2012; 11(3–4):483–492. [PubMed: 21735242]

Christen P, Ito K, Dos Santos AA, Müller R, van Rietbergen B. Validation of a bone loading estimation algorithm for patient-specific bone remodelling simulations. J Biomech. 2013; 46(5):941–948. [PubMed: 23332230]

Christen P, Ito K, Ellouz R, Boutroy S, Sornay-Rendu E, Chapurlat RD, van Rietbergen B. Bone remodelling in humans is load-driven but not lazy. Nat Commun. 2014; 5:4855. [PubMed: 25209333]

Fischer KJ, Jacobs CR, Carter DR. Computational method for determination of bone and joint loads using bone density distributions. J Biomech. 1995; 28(9):1127–1135. [PubMed: 7559684]

Jaroma A, Soininvaara T, Kröger H. Periprosthetic tibial bone mineral density changes after total knee arthroplasty. Acta Orthop. 2016; 87(3):268–273. [PubMed: 27120266]

Mann KA, Miller MA, Pray CL, Verdonschot N, Janssen D. A new approach to quantify trabecular resorption adjacent to cemented knee arthroplasty. J Biomech. 2012; 45(4):711–715. [PubMed: 22227315]

Miller MA, Goodheart JR, Izant TH, Rimnac CM, Cleary RJ, Mann KA. Loss of cementbone interlock in retrieved tibial components from total knee arthroplasties. Clin Orthop Relat Res. 2014; 472(1): 304–313. [PubMed: 23975251]

Miller MA, Terbush MJ, Goodheart JR, Izant TH, Mann KA. Increased initial cement-bone interlock correlates with reduced total knee arthroplasty micro-motion following in vivo service. J Biomech. 2014; 47(10):2460–2466. [PubMed: 24795171]

Ruimerman R, van Rietbergen B, Hilbers P, Huiskes R. A 3-dimensional computer model to simulate trabecular bone metabolism. Biorheology. 2003; 40(1–3):315–320. [PubMed: 12454421]

Ruimerman R, van Rietbergen B, Hilbers P, Huiskes R. The effects of trabecular-bone loading variables on the surface signaling potential for bone remodeling and adaptation. Ann Biomed Eng. 2005; 33(1):71–78. [PubMed: 15709707]

Schulte F, Ruffoni D, Lambers FM, Christen D, Webster DJ, Kuhn G, Müller R. Local mechanical stimuli regulate bone formation and resorption in mice at the tissue level. PLoS One. 2013; 8(4):e62172. [PubMed: 23637993]

Sharkey PF, Lichtstein PM, Shen C, Tokarski AT, Parvizi J. Why are total knee arthroplasties failing today — has anything changed after 10 years? J Arthroplasty. 2014; 29(9):1774–1778. SKAR Annual Report 2016. http://www.myknee.se/pdf/SVK_2016_Eng_1.0.pdf. [PubMed: 25007726]

Srinivasan P, Miller MA, Verdonschot N, Mann KA, Janssen D. Experimental and computational micromechanics at the tibial cement-trabeculae interface. J Biomech. 2016; 49(9):1641–1648. [PubMed: 27079621]

Thompson SM, Yohuno D, Bradley WN, Crocombe AD. Finite element analysis: a comparison of an all-polyethylene tibial implant and its metal-backed equivalent. Knee Surg Sports Traumatol Arthrosc. 2015; 24(8):2560–2566. [PubMed: 26694487]

Weinans H, Huiskes R, Grootenboer HJ. The behavior of adaptive bone-remodeling simulation models. J Biomech. 1992; 25(12):1425–1441. [PubMed: 1491020]

Zhang QH, Cossey A, Tong J. Stress shielding in bone of a bone-cement interface. Med Eng Phys. 2016; 38(4):423–426. [PubMed: 26904919]

Zimmerman WF, Miller MA, Cleary RJ, Izant TH, Mann KA. Damage in total knee replacements from mechanical overload. J Biomech. 2016; 49(10):2068–2075. [PubMed: 27237382]

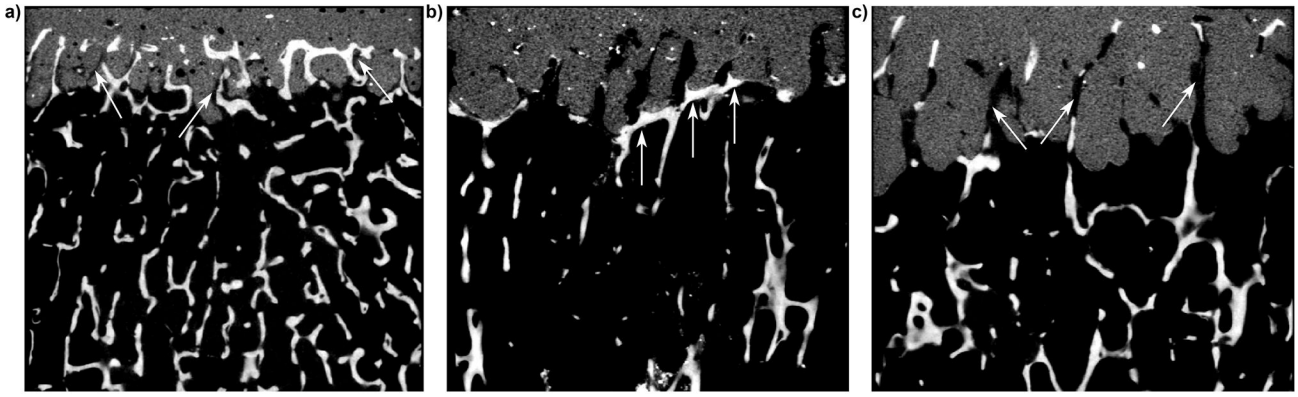

Figure 1.

Specimen morphology a) Minimal resorption (arrows) in interdigitated region b) Pedestal formation (arrows) around cement border with extensive resorption c) Some resorption (arrows) in the interdigitated region.

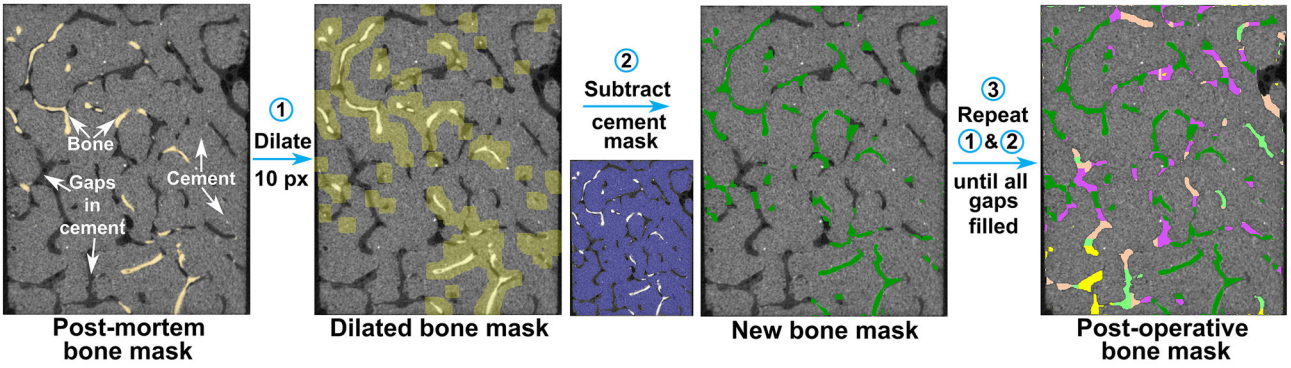

Figure 2.

Segmentation procedure to obtain the post-operative bone mask from the post-mortem bone mask.

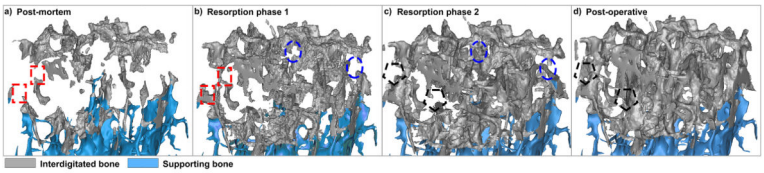

Figure 3.

a) Post-mortem b) resorption phase 1 c) resorption phase 2 and d) post-operative FE models showing the increase of interdigitated bone volume (gray) and connectivity between the four models. Starting with the post-mortem model (a), the volume of interdigitated bone increases in each following model until the post-operative situation (d) is obtained. This is illustrated in the figure by comparing the trabecular structures within each set of geometrical shapes in subsequent images. Supporting bone (blue) volume remains constant but is less visible in each step due to the increasing interdigitated bone.

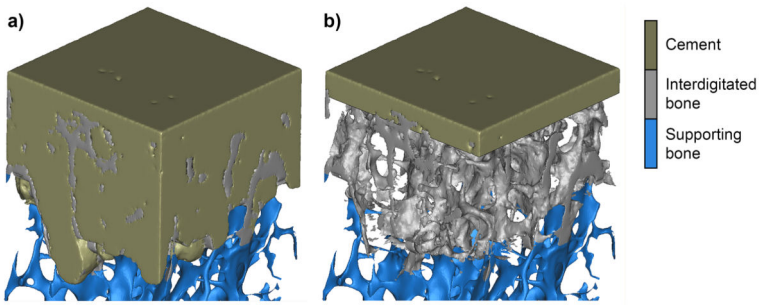

Figure 4.

Pre-operative bone model (b) was obtained by removing the cement layer from the post-operative interface model (a).

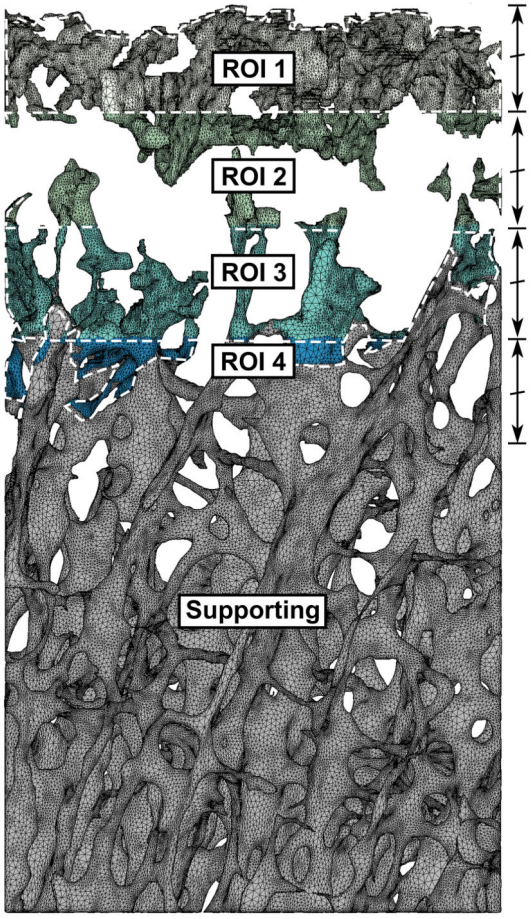

Figure 5.

Post-mortem interdigitated bone for specimen 3 (intermediate resorption) with four regions of interest (ROI 1–4) having equal thickness. Supporting bone was chosen as the layer of bone immediately distal to the interdigitated bone.

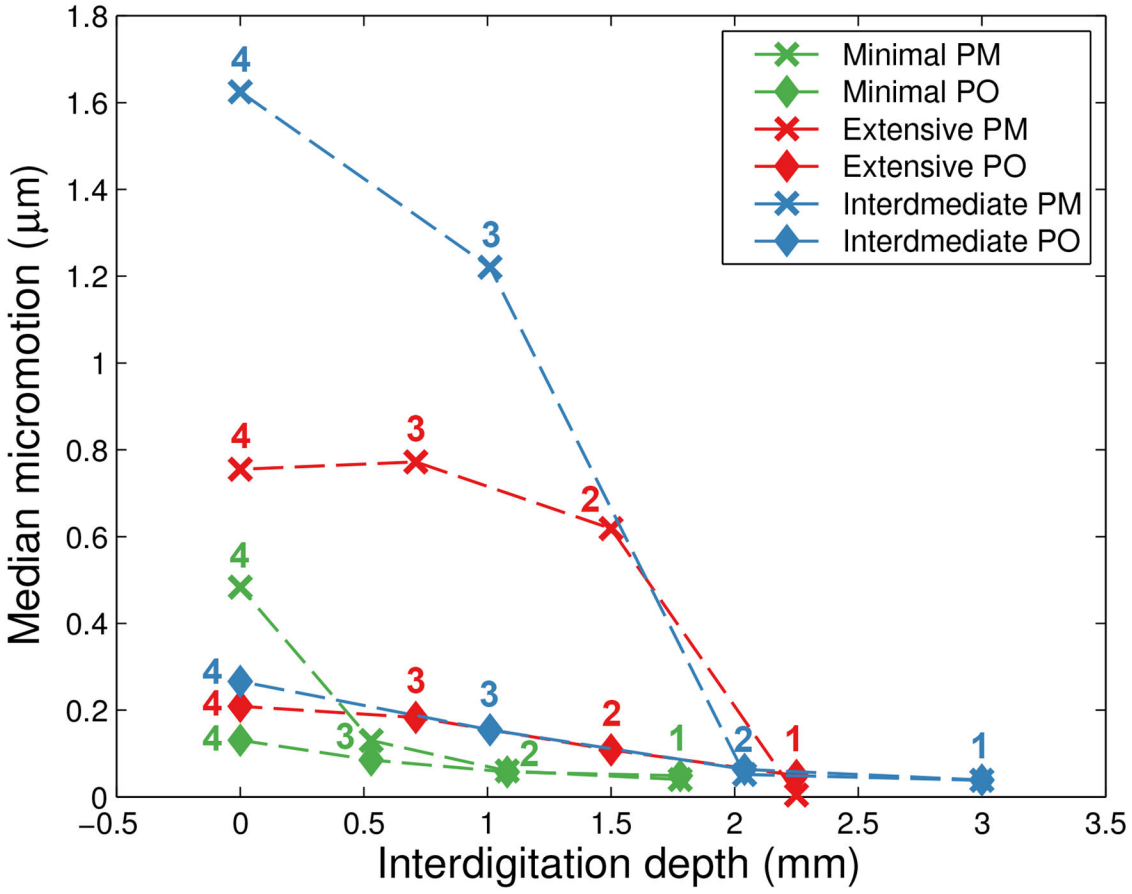

Figure 6.

Distribution of micromotion for the post-mortem (PM) and post-operative (PO) situation for the FE models of all three specimens. Marker numbers correspond to the defined regions of interest in the interdigitated bone of the FE models.

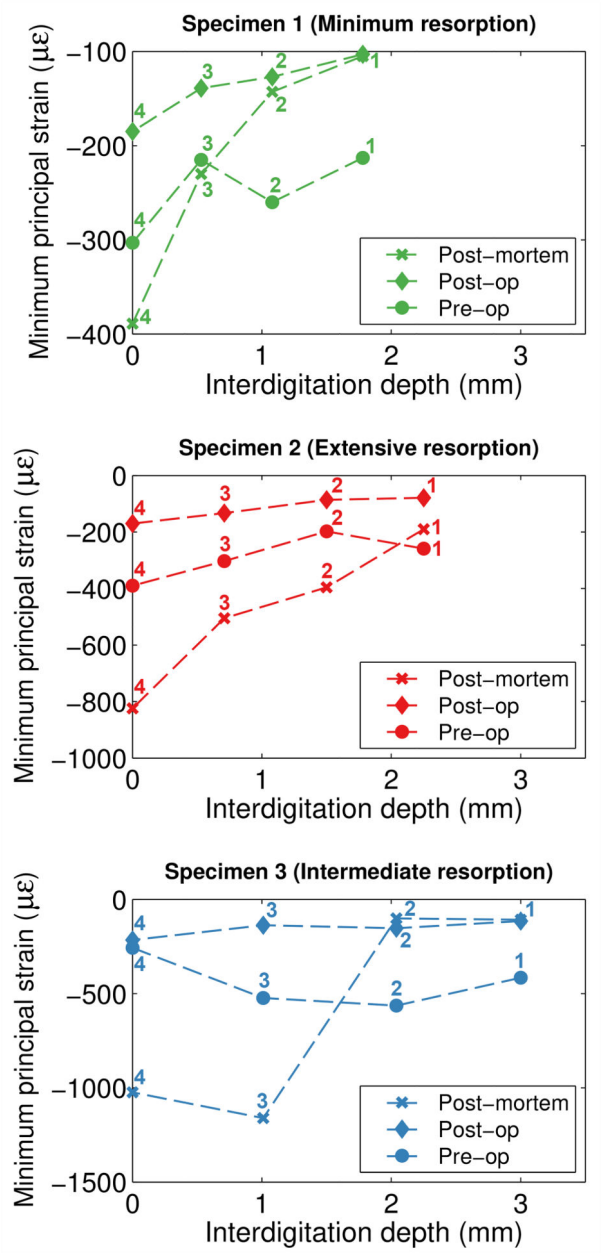

Figure 7.

Interdigitated bone strain as a function of interdigitation depth shows a similar pattern for the FE models of all three specimens.

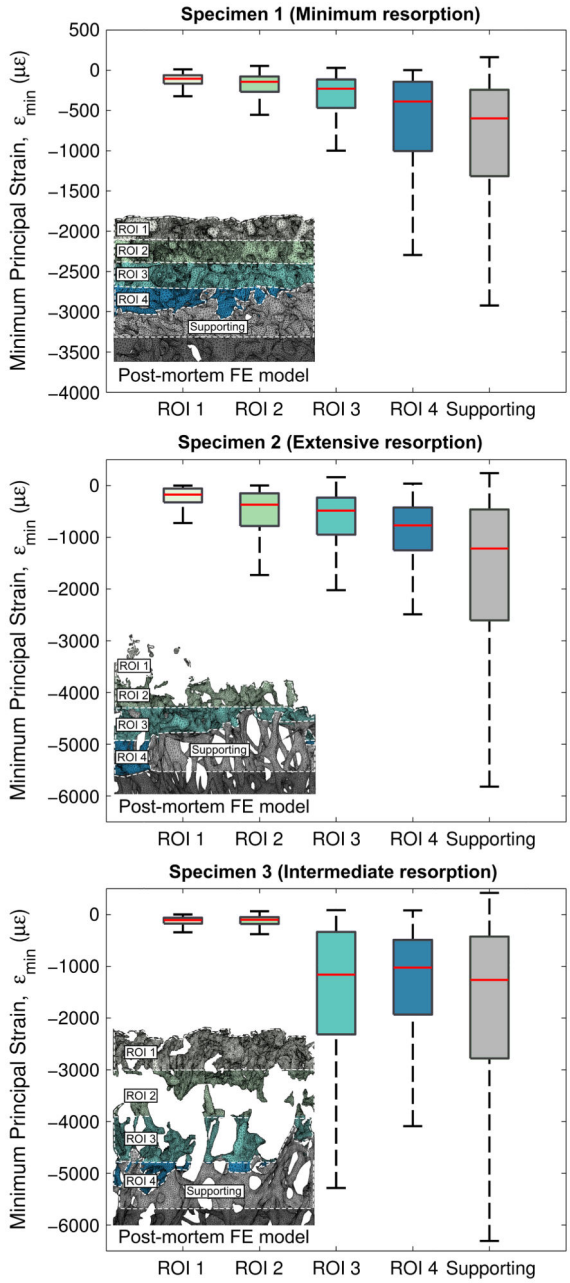

Figure 8.

a) Comparison of strains in interdigitated and supporting bone obtained from the FE models of the three post-mortem specimens. The inlay images show the variation in interdigitated bone between the specimens and the corresponding regions of interest that were used in the boxplots.

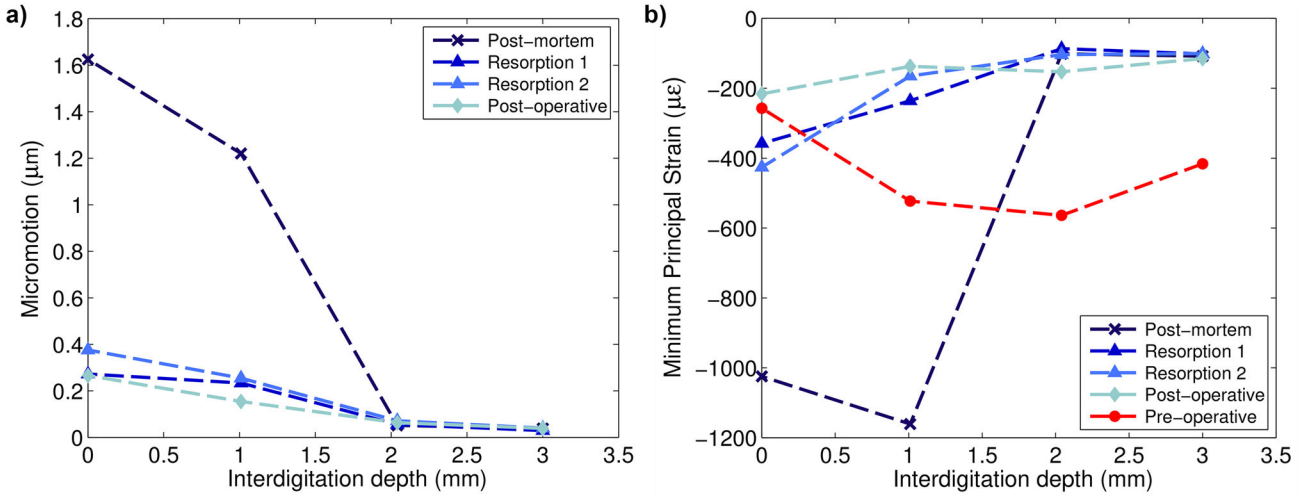

Figure 9.

a) Median micromotion and b) strain distribution for specimen 3 with intermediate resorption for the post-mortem, post-operative and pre-operative situations. Results from two resorption phases between post-operative and post-mortem are also shown.

Table 1

Donor sample and specimen details.

Specimen	Cement penetration depth (mm)	Resorption level	Patient age at time of death (yrs)	Gender	Time in service (yrs)
1	1.8	Minimal	60	Male	5
2	2.3	Extensive	83	Female	6.5
3	3.0	Intermediate	87	Female	3